JOURNAL OF MATERIALS SCIENCE 15 (1980) 2597–2604

Precipitation of NiMo in a Ni-Mo base alloy

H. M. TAWANCY
High Technology Materials Division, Cabot Corporation, Kokomo, Indiana 46901, USA

A study, using electron microscopy and diffraction techniques, was made to characterize a minor second phase present in a corrosion resistant Ni–Mo base alloy (Hastelloy* alloy B containing 27.8 wt% Mo and less than 0.002 wt% C. The effect of second phase distribution in the microstructure on tensile properties and corrosion resistance was determined. The only second phase that could be identified by electron diffraction was found to be the intermetallic NiMo δ phase. It was found that during aging of previously solution treated material, selected grain boundary segments migrate and leave behind NiMo particles. This grain boundary reaction was found to have no detrimental effect on ductility and corrosion resistance.

1. Introduction

The Ni–Mo system forms the basis for a number of Ni-rich alloys which have desirable corrosion resistance in reducing environments provided that Mo remains in solid solution [1–3]. In alloys with a relatively high carbon content, such as the commercial Hastelloy alloy B, dissolution of initially present Mo-rich carbide phases in a weld region and subsequent reprecipitation at grain boundaries of the heat affected zone promote intergranular corrosion [2, 3]. The commercial Hastelloy alloy B has been designed with a minimum carbon content to decrease its tendency to form carbides and consequently an acceptable corrosion resistance in the as-welded condition is retained [3]. The typical heat treatment of this alloy consists of solution treatment at 1065° C followed by quenching to produce an essentially single-phase material. The resulting microstructure is similar to that of Hastelloy alloy B and contains a second phase dispersed throughout the α-f c c solid solution matrix. Riddle and Gray [4] have identified the phase present in Hastelloy alloy B to be a carbide of the form M_6C; however, Claussing *et al.* [5] speculated that this could be the intermetallic NiMo and/or a mixture of carbides. Flint [2] has reported that in Ni–Mo alloys containing up to 30 wt% Mo and 5 wt% Fe, no carbide phases are present as long as the carbon content is ⩽ 0.005 wt%. However, a second phase was still present in these alloys but in too small an amount to be identified by normal extraction and X-ray diffraction techniques. More recently, a carbide of the form $M_{12}C$ has been reported to exist in the Ni–Mo–C ternary system [6, 7] and silicon was found to play a significant role in stabilizing this carbide in Hastelloy alloy N [8]. On the other hand, it was found that other alloying elements, particularly Fe, cause a shift in the phase field where the solid solution and NiMo can coexist toward a lower Mo content relative to the binary system [9]. Lei [10] has recently identified NiMo in a Ni–27.9 wt% Mo–4.4 wt% Fe alloy using energy dispersive X-ray analysis.

It appears from the findings discussed above that the exact nature of the phase, or phases, present is a sensitive function of chemical composition, particularly of the carbon content, iron content and the content of carbide stabilizing elements such as silicon and vanadium. In order to better control the behaviour of these alloys, it is then important to correlate chemical composition with the nature of the phase, or phases, present, and to determine the corresponding effect on mechanical properties and corrosion resistance. The objective of this investigation was to characterize the second phase of Hastelloy alloy B, containing less than 0.002 wt% C, and

*Hastelloy is a registered trademark of the Cabot Corporation.

0022–2461/80/102597–08 $02.80/0

TABLE I Chemical analysis of the alloy used

Element	Ni	Mo	Fe	Cr	Co	Si	V	N	O	C
Concentration (wt %)	68.50	27.79	0.87	0.69	<0.01	<0.02	<0.01	0.006	0.005	<0.002

to determine the effect of the phase distribution in the microstructure on the tensile properties and on corrosion resistance.

2. Experimental procedure

The alloy used in the present investigation was of commercial grade and provided in the wrought condition as sheets 1.75 mm thick. The result of chemical analysis is given in Table I.

Table II summarizes the results of various characterization tests performed on the as-received material.

In order to examine the response of the second phase to high temperature exposure and subsequent aging at lower temperatures, specimens were subjected to the following heat treatment schedule under argon atmosphere: (a) solution treatment at 1150° C for 2 hours followed by ice water quenching and (b) subsequent aging at 1065° C, 1010° C, 955° C and 900° C for between 1 and 3 hours followed by ice water quenching. These temperatures were chosen to avoid complications from the ordering reactions which occur at lower temperatures [11]. The second phase was investigated using electron diffraction and microscopy techniques. Attempts to extract this second phase for X-ray diffraction analysis were made but were unsuccessful because of the small volume fraction present. Thin foils were prepared from as-received, as-quenched, and aged specimens by the jet polishing technique in a solution consisting of 30 vol% HNO_3, balance methanol at about −30° C. All the foils were examined using a Philips 300EM electron microscope operating at 100 kV; thicker regions were preferentially examined to increase the chance of locating second phase particles. Specimens for light optical metallography were etched in a solution containing 80% conc. HCl to 20% 15 mol% chromic acid. Qualitative X-ray microanalysis of second phase particles was performed in an ISI-100 scanning electron microscope using an Ortec energy dispersive system. Corrosion tests were performed in 11 mol% boiling HCl for three 96-hour periods, and the penetration rate extrapolated to $\mu m\,year^{-1}$ was determined from the weight loss.

TABLE II Characteristic properties of the as-received material

Property	Experimentally determined value
Volume fraction of second phase*	0.01
Diameter of second phase particles	0.5–7.0 μm
Lattice constant of the f c c matrix†	0.361 nm
0.2% Yield strength	370 MPa
Ultimate tensile strength	920 MPa
Tensile elongation (50.8 mm gauge length)	55.6%
Corrosion penetration rate in 20% boiling HCl	3 $\mu m\,year^{-1}$

*Measured by sytematic count-grid points
†Measured by X-ray diffraction

3. Results and discussion

3.1. Light optical metallography and qualitative X-ray microanalysis

Fig. 1 is a representative set of light optical micrographs showing the effect of the heat treatment schedule described above on the gross microstructural features. It can be seen that, as a result of solution treatment at 1150° C, the second phase partially dissolved in the matrix, the grains of which have grown considerably. Subsequent aging at lower temperatures caused grain boundary precipitation of an increasing amount as the aging temperature decreased. The grain boundary precipitate assumed a lamellar morphology which became more pronounced as the aging temperature decreased with an associated migration of grain boundary segments (compare Figs. 1c and d). These are typical features of a discontinuous precipitation mode and, hence, suggest a reaction controlled by grain boundary diffusion [12, 13]. Qualitative X-ray microanalysis performed on second-phase particles inside the grains and at grain boundaries of as-quenched and aged specimens showed these particles to be depleted in Ni and enriched in Mo relative to the matrix with no detectable segregation of other elements present

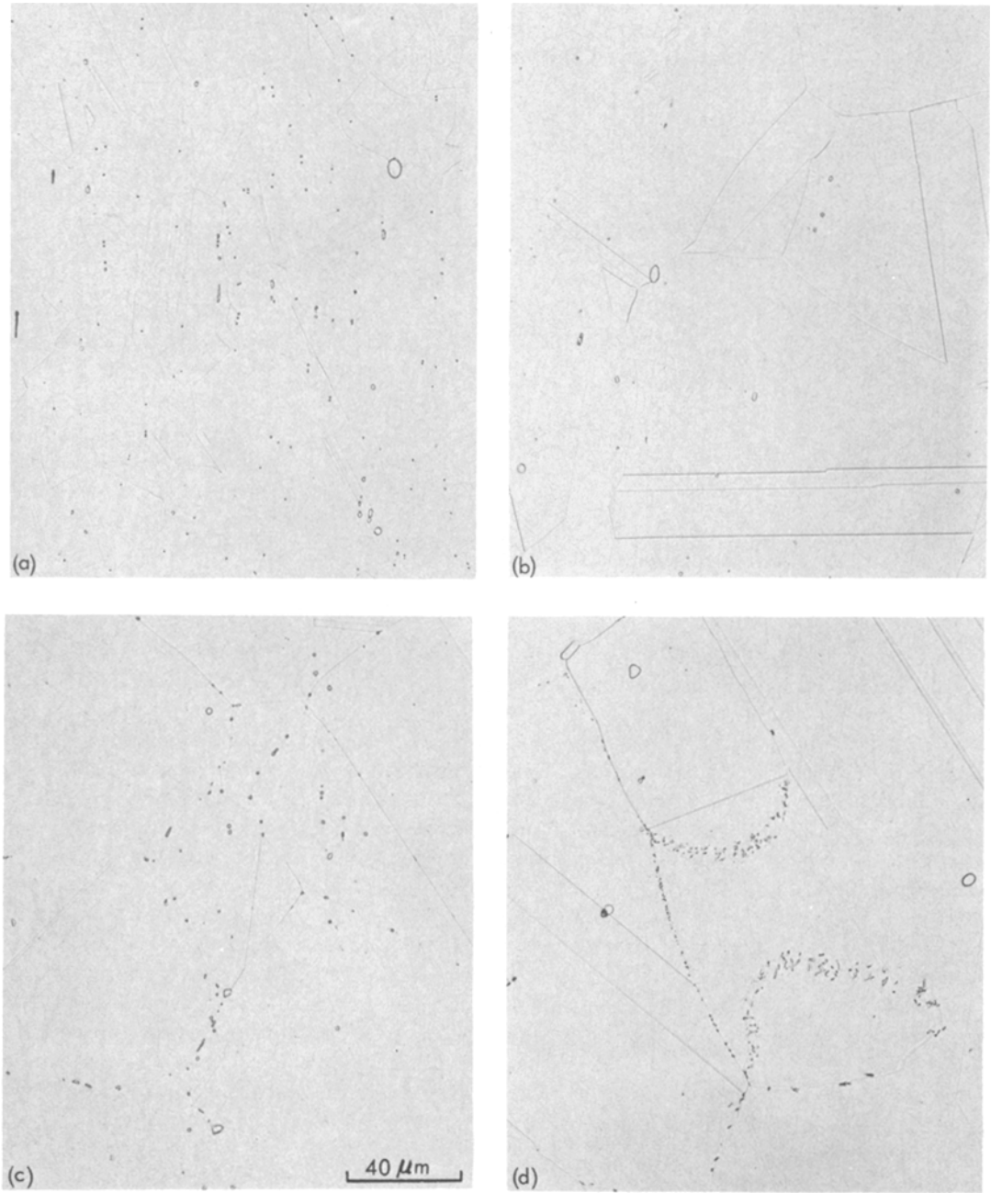

Figure 1 Light optical micrographs showing the effect of heat treatment on the distribution of second phase in the microstructure: (a) As-received; (b) Solution treated at 1150° C for 2 hours and then ice water quenched; (c) Same treatment as in (b) plus 2 hours aging at 1065° C; (d) Same treatment as in (b) plus 2 hours aging at 900° C.

within the resolution limit of the equipment. A typical example of such an analysis is shown in Fig. 2. The observation that selected grain boundary segments migrate suggests that precipitation only occurs at regions of large grain misorientation. This is also evident from the observation that no precipitates formed at the $\{1\ 1\ 1\}_{fcc}$ annealing twin boundaries.

3.2. Electron diffraction and microscopy

Fig. 3 shows the results of a dark-field microscopy experiment performed on a second-phase particle,

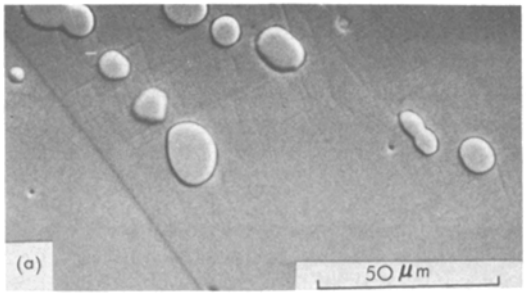

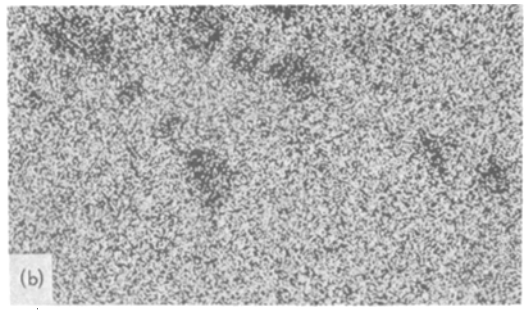

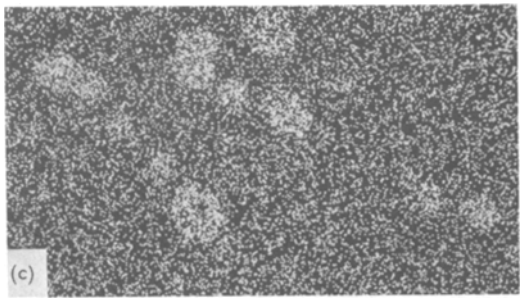

Figure 2 Qualitative X-ray microanalysis of a second-phase particle. (a) Scanning electron micrograph; (b) X-ray image of Ni distribution; (c) X-ray image of Mo distribution.

and Fig. 4 shows a set of selected area diffraction patterns derived from individual particles at different tilts. The d-spacings and interplanar angles as measured from these diffraction patterns could uniquely be ascribed to the intermetallic NiMo within an estimated error of ± 1% or better. The crystal structure of NiMo, determined by Shoemaker and Shoemaker [14], was found to possess a complex ordered orthorhombic pseudotetragonal cell with unit cell dimensions $a_0 = b_0 = 0.9108$ nm and $c_0 = 0.8852$ nm. The observed absence of (1 0 0), (3 0 0), (5 0 0), . . . (n 0 0) reflections is in agreement with X-ray diffraction data of Shoemaker and Shoemaker [14]. The observation in Fig. 3 that a complete zone of NiMo particle (inside a grain) is superimposed on that of the matrix suggests a crystallographic orientation relationship such that

$$[0\,\bar{4}\,1]_{\mathrm{NiMo}} \parallel [0\,1\,1]_{\mathrm{fcc}} \quad (1)$$

and

$$(2\,1\,4)_{\mathrm{NiMo}}\ 2^\circ \text{ from } (\bar{1}\,1\,\bar{1})_{\mathrm{fcc}}. \quad (2)$$

The only second phase particles that could be located and analysed by electron diffraction had diameters of between about 0.5 and 2 μm and therefore, it cannot be claimed that all of the second phase investigated is NiMo. Since the larger particles constitute a very small fraction of the total, it can be concluded that, at least, most of the second phase is NiMo. The observed discontinuous precipitation of NiMo upon aging indicates that this process is controlled by lateral diffusion of Mo along grain boundaries. Fig. 5 is an electron micrograph showing a grain boundary NiMo particle in specimen aged for 1 hour at 955° C. The reaction occurring at the grain boundary can be expressed as

$$\alpha[27.8\ \text{wt\% Mo}] \rightarrow \alpha''[(27.8 - x)\text{wt\% Mo}] + \delta\ \text{NiMo}. \quad (3)$$

That is, the supersaturated solid solution α decomposes into α′, the Mo content of which is closer to the equilibrium concentration at the respective temperature. According to the binary Ni–Mo phase diagram, the solid solubilities of Mo in Ni at 1065° C, 1010° C, 955° C and 900° F are 33.1 wt%, 31.9 wt%, 30.6 wt%, and 29.3 wt%, respectively [15]. In view of the small amount of NiMo present, x in the above equation is expected to be of the order of a fraction of a per cent. Therefore, the above grain boundary reaction is not expected to result in a grain boundary zone that is significantly depleted in Mo. The observed response of NiMo to solution treatment, and subsequent aging, suggests that it had formed, and had assumed the morphology observed in, as-received material during thermomechanical processing. This consisted of hot forging and rolling in the temperature range between 1230° C and 955° C.

3.3. Effect of grain boundary precipitation of NiMo on tensile properties and corrosion resistance

Table III shows the effect of aging for 2 hours at different temperatures on room temperature tensile properties and corrosion penetration rates.

It can be concluded from the data of Tables II

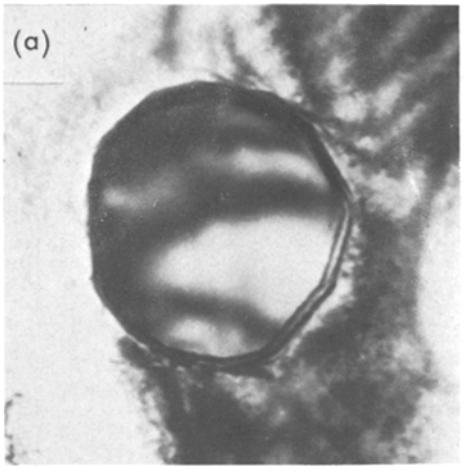

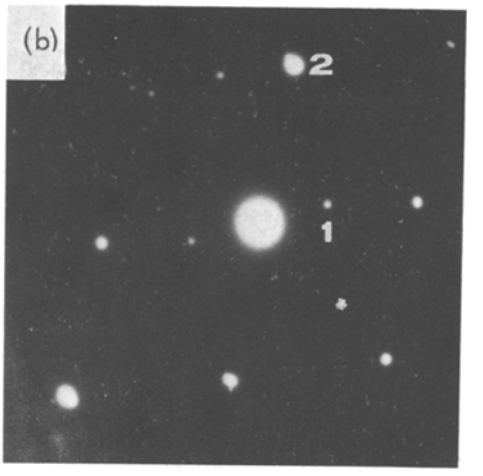

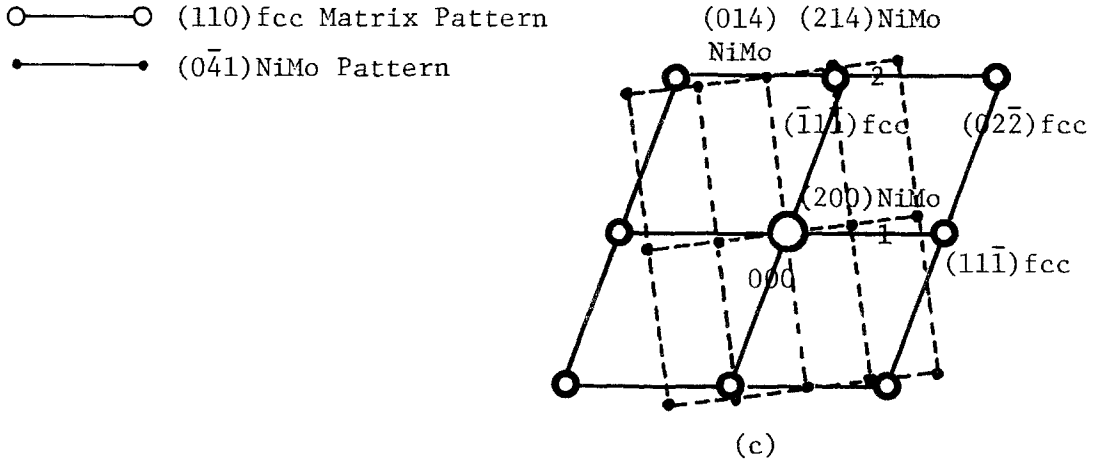

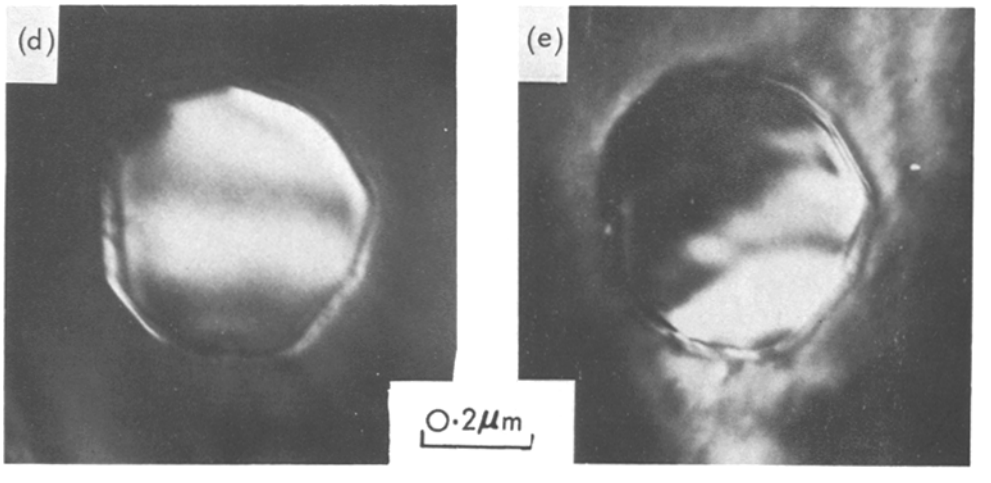

Figure 3 Transmission electron microscopy and diffraction of a second phase particle. (a) Bright-field image; (b) Selected area electron diffraction pattern derived from the particle and surrounding matrix; (c) Interpretation of the diffraction pattern; (d) Dark-field image formed by spot 1; (e) Dark-field image formed by spot 2 (spot 2 represents nearly superimposed particle and matrix spots.

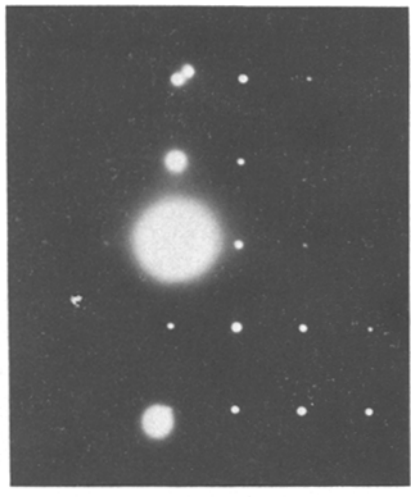

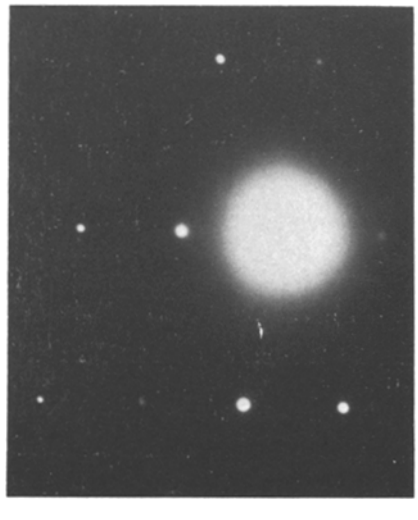

Figure 4 Electron diffraction patterns of second-phase particles indexed in terms of the NiMo structure: (a) $[1\bar{1}\bar{2}]$; (b) $[0\bar{1}2]$; (c) $[\bar{3}14]$.

Figure 5 Bright-field electron micrograph showing a grain boundary NiMo particle (specimen aged for 1 hour at 955° C).

and III that grain boundary precipitation of NiMo neither embrittled the grain boundaries nor did it promote intergranular corrosion. This can be explained in terms of a boundary product, α', whose Mo content is very close to that of the parent α. Therefore, the grain boundary reaction does not create a boundary zone where slip and corrosion can occur preferentially. This contrasts the damaging effect of the grain boundary precipitation of carbides, particularly on corrosion resistance. Although it may be argued that this difference is only due to different amounts of precipitates in each case, other factors such as (a) the mechanism of precipitation and (b) the nature of grain boundary, i.e. whether high or low angle may significantly affect the composition profile near grain boundaries. The exact role of these parameters must await further investigation.

4. Conclusions

A study involving electron microscopy and diffraction techniques was made to characterize a minor second phase present in a Ni–Mo base alloy (Hastelloy alloy B) and to determine the effect of the phase distribution in the microstructure on tensile properties and corrosion resistance. The following conclusions which only pertain to the particular heat investigated can be drawn:

(a) The only second phase that could be detected by electron diffraction is the intermetallic NiMo δ phase.

(b) Solution treatment and subsequent aging at lower temperatures causes selected segments of grain boundaries to migrate and leave behind NiMo particles.

(c) The grain boundary reaction has no detrimental effect on ductility and corrosion resistance.

References

1. L. V. GERNETS, S. A. GOLOVANENKO and R. V. SVISTUNOVA, *Metalloveniei Temicheskaya Obrabotka Metallov* **2** (1975) 47. Translation by Plenum publishing Corporation, New York, 1975, p. 144.
2. G. N. FLINT, *J. Inst. Met.* 87 (1958–59) 303.
3. F. G. HODGE and R. W. KIRCHNER, *Mater. Performance* **15** (1976) 40.
4. J. R. RIDDLE and R. J. GRAY, "Metallography and Aging Characteristics of Hastelloy-B" (Oak Ridge National Laboratory Report No. 2496, Oak Ridge, Tennessee 1964).
5. R. E. CLAUSSING, P. PATRIARCA and W. D. MANLY, *Trans. ASM* **51** (1959) 123.
6. A. C. FRACKER and H. H. STADELAMAIR, *Trans. AIME* **245** (1969) 847.
7. C. P. HEIJWEGEN and G. D. RIECK, *Met. Trans.* **4** (1973) 2159.
8. J. M. LEITNAKER, G. A. POTTER, D. J. BRADLY, J. C. FRANKLIN and W. R. LAING, *ibid.* **9A** (1978) 397.
9. W. E. NOREM, "An Investigation of the Nickel-Rich Alloys Containing Molybdenum and Iron", M.Sc. Thesis, The University of Tennessee, Knoxville,

TABLE III The effect of aging for 2 hours, at different temperatures, on room temperature tensile properties and corrosion penetration rates

Aging temperature (° C)	0.2% yield strength (MPa)	Ultimate tensile strength (MPa)	Tensile elongation (%)	Corrosion penetration rate (μm year)
1065	343	825	63	3.0
1010	342	820	63	2.90
955	343	825	64	2.80
900	343	825	63	2.90

Tennessee, USA, 1963).
10. T. S. LEI, "The Effect of 0-8 Weight Per Cent Iron on Transformation of a α Phase Ni–Mo–Fe Alloys with Ni:Mo Ratio Equal 4:1", Ph.D. Thesis, The University of Tennessee, Knoxville, Tennessee, USA, (1979).
11. G. VAN TENDELEO, *Mater. Sci. Eng.* **26** (1976) 209.
12. D. TURNBULL and K. N. TU, in "Phase Transformations" edited by H. I. Aaronson (American Society for Metals, Metals Park, Ohio, 1970) p. 487.
13. C. S. SMITH, *Trans. ASM* **45** (1953) 562.
14. C. B. SHOEMAKER and D. P. SHOEMAKER, *Acta Cryst.* **16** (1963) 997.
15. M. HANSEN, "Constitution of Binary Alloys" (McGraw Hill, New York, 1958) p. 968.

Received 25 January and accepted 13 March 1980.